Scientific Research Publishing

World Journal of Condensed Matter Physics, 2023, 13, 14-39
https://www.scirp.org/journal/wjcmp
ISSN Online: 2160-6927
ISSN Print: 2160-6919

Degenerate States in Nonlinear Sigma Model with SU(2) Symmetry

Tomo Munehisa

Faculty of Engineering, University of Yamanashi, Kofu, Japan
Email: munehisa8tomo@gmail.com

How to cite this paper: Munehisa, T. (2023) Degenerate States in Nonlinear Sigma Model with SU(2) Symmetry. *World Journal of Condensed Matter Physics*, **13**, 14-39.
https://doi.org/10.4236/wjcmp.2023.131002

Received: November 16, 2022
Accepted: February 25, 2023
Published: February 28, 2023

Abstract

Entanglement in quantum theory is a peculiar concept to scientists. With this concept we are forced to re-consider the cluster property which means that one event is irrelevant to another event when they are fully far away. In the recent works we showed that the quasi-degenerate states induce the violation of cluster property in antiferromagnets when the continuous symmetry breaks spontaneously. We expect that the violation of cluster property will be observed in other materials too, because the spontaneous symmetry breaking is found in many systems such as the high temperature superconductors and the superfluidity. In order to examine the cluster property for these materials, we studied a quantum nonlinear sigma model with U(1) symmetry in the previous work. There we showed that the model does have quasi-degenerate states. In this paper we study the quantum nonlinear sigma model with SU(2) symmetry. In our approach we first define the quantum system on the lattice and then adopt the representation where the kinetic term is diagonalized. Since we have no definition on the conjugate variable to the angle variable, we use the angular momentum operators instead for the kinetic term. In this representation we introduce the states with the fixed quantum numbers and carry out numerical calculations using quantum Monte Carlo methods and other methods. Through analytical and numerical studies, we conclude that the energy of the quasi-degenerate state is proportional to the squared total angular momentum as well as to the inverse of the lattice size.

Keywords

Quantum Nonlinear Sigma Model, SU(2): Special Unitary Group in Two Dimensions, Cluster Property, Spontaneous Symmetry Breaking, Degenerate States, Spin-Weighted Harmonics

1. Introduction

We find quite long history in the study of the quantum nonlinear sigma model

(QNLSM) [1] [2] [3] [4], since it has been derived as the effective model for two-dimensional Heisenberg antiferromagnets [5] [6] [7]. Another remarkable application of this model has been made to particle physics [8] [9] [10], where it is called chiral Lagrangian. Using this application we have met with fruitful results on hadron physics [11]. Also this model is deeply connected with quantum mechanics of the constrained particle [12] [13], or of the particle with the attractive potential induced by the geometry [14] [15]. The reason why QNLSM has been employed in such wide fields of physics is that the model realizes the symmetry by the minimum degrees of freedom when the continuous symmetry is spontaneously broken.

Our purpose in this paper is to show that QNLSM exhibits the quasi-degenerate states (QDS) which induce the violation of the cluster decomposition [16], or the cluster property [17]. The cluster property means that there is no relation between two events occurring infinitely apart from each other. This property has been considered to be fundamental in physics because, based on this property, we can observe the event locally and the result is irrelevant to those of other events which occur at the long distances. In previous works [18] [19] [20] we studied this property using Heisenberg spin model on the square lattice [21], which has been a model for many materials [22] [23]. Active studies in the many-body systems [17] [24] [25] [26] and in quantum field theory [27] [28] including QCD [29] [30], on the other hand, are made on the cluster property about somewhat special models which are too theoretical.

In our study [18] [19] [20] we found the cluster property violation in the system on a lattice with spontaneous symmetry breaking (SSB). The key observation is that there exist the quasi-degenerate states with energy E_{n_Q} which is the lowest one for a quantum number n_Q related to the symmetry. In the spin systems of N_s sites it has been well known that the energy gap $E_{n_Q} - E_0$ is proportional to n_Q^2 / N_s [21].

In a previous work [31] we studied QDS of QNLSM with U(1) symmetry. The reason on this model is that it is the effective model for the superconductors and the super-fluidity. We have investigated a quantum model defined on a lattice using the Weyl representation [32] [33] [34] with discrete and finite variables. In addition, we adopted the representation where the kinetic term is diagonalized. Then we carried out analytical discussions so that we could implement numerical method to calculate the energy with the fixed value of n_Q. From numerical results, which are obtained by the diagonalization, stochastic state selection method [35]-[42] and quantum Monte Carlo methods [43] [44] [45], we have observed the energy gap which is composed of a term n_Q^2 / N_s and its correction terms.

In the present work we study QNLSM with SU(2) symmetry. The formulation in this case is more complicated since the conjugate variables to the angle variables, θ_k and ϕ_k at each site k, cannot be defined. In order to avoid this difficulty, we employ the Hamiltonian with the potential term given by the angle variables themselves. For the kinetic term, on the contrary, we use the squared

angular momentum which is given by the quantum numbers l_k and m_k. Following to the case of U(1) symmetry, we adopt the representation that the kinetic term is diagonalized. Then we develop numerical methods including quantum Monte Carlo methods. Note that this method is indispensable, because we cannot fix the quantum number directly in ordinary Monte Carlo methods based on the path integral. Our conclusion is that the energy of the quasi-degenerate state shows $J(J+1)/N_s$ dependence, where J denotes the total angular momentum of the system.

Let us describe the plan of this paper. In the next section we define our QNLSM on the square lattice with SU(2) symmetry. The Hamiltonian of our model is the sum of the kinetic term and the potential term. The kinetic term at each site is given by the square of the total angular momentum operator, where we fix the strength of the kinetic term to be 1. The potential term, whose strength is denoted by B, is formed by the angular variables at neighboring sites of a link. Also we explicitly express the potential term by the quantum numbers l_k and m_k at the site k.

In Section 3 we theoretically discuss the cases for large B as well as small B of our Hamiltonian. In the first subsection we derive an effective Hamiltonian when B is large. Note that it is a non-trivial task to find the conserved operator, which is the sum of the angular momentum operators at each site, in the large limit of B. In the next subsection we show analytical results on energy for small B. In this case the discussion is straightforward because we can apply the perturbation theory of the potential to the unperturbed Hamiltonian with $B=0$.

Section 4 is devoted to preparations for numerical study. First, we examine the max value of l, $l_{\max}$, for the numerical calculations. Then parameters β and l_t used in quantum Monte Carlo methods are also determined. In Section 5 we show our numerical results on lattices with $N_s=2,8,16,36$ and 64 sites. In the first subsection our discussion for large B is justified by numerical results of $N_s=2$, where many excited states are calculated. The results on the $N_s\geq 8$ lattices are presented in the next subsection. There we employ stochastic state selection (SSS) method [35]-[42] for the $N_s=8$ lattice, while calculations for $N_s=16,36$ and 64 lattices are carried out by quantum Monte Carlo methods [43] [44] [45].

Finally we summarize our work and discuss future studies in the last section. Here we point out that the Hamiltonian for quite large B shows the spin weighted harmonics for SU(2) symmetry [46].

We add two subsections in Appendix. In the first subsection, we present details to derive the effective Hamiltonian for large B, which is much complicated. Since this Hamiltonian has the spin weighted harmonics, we are led to a constraint on the quantum numbers. In the second subsection we show that this constraint is given by the eigen function of the spin weighted harmonics.

Since many symbols and variables are used in our paper, we list them in **Table 1** for convenience.

Table 1. Symbols or variables used in our work. The third column denotes the equation number, if any, where the symbol or the variable is defined.

Symbol	Meaning	Def. Equation
$\hat{H}$	Hamiltonian of our model	(1)
$\hat{T}$	Kinetic term of $\hat{H}$	(2)
$\hat{V}_B$	Potential term of $\hat{H}$	(3)
B	Strength of $\hat{V}_B$	(3)
$\hat{V}_{kk'}$	Local interaction of $\hat{V}_B$	(4)
θ_k, ϕ_k	Angle variables at site k	
$\lvert l_k, m_k \rangle$	State of quantum numbers l, m at site k	(5)
$\hat{L}_{\alpha,k}$	Angular momentum operators	
N_s	Total number of sites	
θ	Average angle of θ_k	(11)
ϕ	Average angle of ϕ_k	(11)
a_{jk}	Matrix element of orthogonal trans.	(13)
ξ_j	Angle by orthogonal trans. of θ_k	(14)
χ_j	Angle by orthogonal trans. of ϕ_k	(14)
$\hat{L}_{\xi,\alpha,k}$	Operators by orthogonal trans. of $\hat{L}_{\alpha,k}$	(19)
$\tilde{\xi}_j$	Variable changed from ξ_j	(22)
η_j	Variable changed from χ_j	(22)
$\hat{L}_{A,\pm}$	Effective op. of angular mo. with ± compo.	(21)
$\hat{L}_{\phi}$	Effective op. of angular mo. with z compo.	(26)
$\hat{H}_A$	Effective Hamiltonian for large B	(28)
$\lvert \Psi_0 \rangle$	Ground state for $B = 0$	(30)
J	Quantum number of total angular momentum	
E_J	Lowest energy of J	
n_{link}	Link number of one site	
$l_{\max}$	Maximum of l in numerical calculations	Section 4.1
$\hat{H}_{A,2}$	Effective Hamiltonian of two particles	(46)

2. Quantum Nonlinear Sigma Model

We define the Hamiltonian of our model using only angle variables θ_k's and ϕ_k's on sites. The Hamiltonian we start with is given by

$$\hat{H} \equiv \hat{T} + \hat{V}_B, \tag{1}$$

$$\hat{T} \equiv \sum_{k=0}^{N_s-1} \hat{T}_k,\ \hat{T}_k \equiv \left(\hat{\vec{L}}_k\right)^2 = -\left(\frac{\partial^2}{\partial\theta_k^2} + \cot\theta_k \frac{\partial}{\partial\theta_k} + \csc^2\theta_k \frac{\partial^2}{\partial\phi_k^2}\right), \tag{2}$$

$$\hat{V}_B \equiv B\sum_{(k,k')} \hat{V}_{kk'}\ \ (B>0), \tag{3}$$

$$\hat{V}_{kk'} \equiv 1 - \cos\theta_k\cos\theta_{k'} - \sin\theta_k\sin\theta_{k'}\cos\left(\phi_k - \phi_{k'}\right). \tag{4}$$

Here (k,k') denotes a pair of neighboring sites of a link and N_s is the total number of sites on the lattice. Note that we have included a constant term 1 into $\hat{V}_{kk'}$ so that it becomes zero when $\theta_k = \theta_{k'}$ and $\phi_k = \phi_{k'}$.

The state at each site k is described by the quantum numbers l_k and m_k. Therefore the basis state of the lattice is given by

$$\left|\left\{\left(l_k m_k\right)\right\}\right\rangle \equiv \prod_{k=0}^{N_s-1} \left|l_k m_k\right\rangle,$$

$$\left(\hat{\vec{L}}_k\right)^2 \left|l_k m_k\right\rangle = \left|l_k m_k\right\rangle l_k\left(l_k+1\right),\ \hat{L}_{z,k}\left|l_k m_k\right\rangle = \left|l_k m_k\right\rangle m_k. \tag{5}$$

Next we present the matrix elements of the potential term $\hat{V}_{kk'}$, which are defined by

$$V\left(l_k' m_k'; l_{k'}' m_{k'}' \,|\, l_k m_k; l_{k'} m_{k'}\right) \equiv \left\langle l_k' m_k'; l_{k'}' m_{k'}' \left|\hat{V}_{kk'}\right| l_k m_k; l_{k'} m_{k'}\right\rangle,$$

$$\left|l_k m_k; l_{k'} m_{k'}\right\rangle \equiv \left|l_k m_k\right\rangle\left|l_{k'} m_{k'}\right\rangle. \tag{6}$$

For the matrix elements of $\hat{V}_{kk'}$, we calculate $\left\langle l', m'\left|\cos\theta\right|l, m\right\rangle$ and $\left\langle l', m'\left|\sin\theta \mathrm{e}^{\pm i\phi}\right|l, m\right\rangle$. For these calculations, we use the spherically harmonic polynomials $Y_l^m(\theta,\phi)$ and the equations between three Legendre polynomials $P_l^m(x)$, which are given by

$$\left(2l+1\right)xP_l^m\left(x\right) = \left(l+1-m\right)P_{l+1}^m\left(x\right) + \left(l+m\right)P_{l-1}^m\left(x\right),$$

$$P_{l+1}^{m+1}\left(x\right) - P_{l-1}^{m+1}\left(x\right) - \left(2l+1\right)\sqrt{1-x^2}P_l^m\left(x\right) = 0. \tag{7}$$

Then we obtain the results, which are summarized in Table 2.

Now we consider to calculate the matrix elements of $\hat{V}_{12}$ for two particles defined by

$$\begin{aligned}\hat{V}_{12} &\equiv 1 - \cos\theta_1\cos\theta_2 - \sin\theta_1\sin\theta_2\cos\left(\phi_1 - \phi_2\right)\\ &= 1 - \cos\theta_1\cos\theta_2 - \sin\theta_1\sin\theta_2 \cdot \frac{1}{2}\left\{\mathrm{e}^{i(\phi_1-\phi_2)} + \mathrm{e}^{-i(\phi_1-\phi_2)}\right\}.\end{aligned} \tag{8}$$

We adopt a notation on the state of two particles.

$$\left|l_1, l_2; m_1, m_2\right\rangle \equiv \left|l_1, m_1\right\rangle\left|l_2, m_2\right\rangle. \tag{9}$$

Then the matrix elements of the potential $\hat{V}_{12}$ are given by

Table 2. Non-zero matrix elements of $\cos\theta$ and $\sin\theta e^{\pm i\phi}$.

$\hat{O}$	l'	m'	$\langle l'm'\vert\hat{O}\vert lm\rangle$
$\cos\theta$	$l+1$	m	$\sqrt{\frac{(l-m+1)(l+m+1)}{(2l+1)(2l+3)}}$
$\cos\theta$	$l-1$	m	$\sqrt{\frac{(l-m)(l+m)}{(2l-1)(2l+1)}}$
$\sin\theta e^{i\phi}$	$l+1$	$m+1$	$-\sqrt{\frac{(l+m+1)(l+m+2)}{(2l+1)(2l+3)}}$
$\sin\theta e^{i\phi}$	$l-1$	$m+1$	$\sqrt{\frac{(l-m-1)(l-m)}{(2l-1)(2l+1)}}$
$\sin\theta e^{-i\phi}$	$l+1$	$m-1$	$\sqrt{\frac{(l-m+1)(l-m+2)}{(2l+1)(2l+3)}}$
$\sin\theta e^{-i\phi}$	$l-1$	$m-1$	$-\sqrt{\frac{(l+m-1)(l+m)}{(2l-1)(2l+1)}}$

$$\begin{aligned}
&\langle l_1', l_2'; m_1', m_2'\vert\hat{V}_{12}\vert l_1, l_2; m_1, m_2\rangle = \langle l_2', m_2'\vert\langle l_1', m_1'\vert\hat{V}_{12}\vert l_1, m_1\rangle\vert l_2, m_2\rangle \\
&= \langle l_1', m_1'\vert l_1, m_1\rangle\langle l_2', m_2'\vert l_2, m_2\rangle - \langle l_1', m_1'\vert\cos\theta_1\vert l_1, m_1\rangle\langle l_2', m_2'\vert\cos\theta_2\vert l_2, m_2\rangle \\
&\quad -\frac{1}{2}\langle l_1', m_1'\vert\sin\theta_1 e^{i\phi_1}\vert l_1, m_1\rangle\langle l_2', m_2'\vert\sin\theta_2 e^{-i\phi_2}\vert l_2, m_2\rangle \\
&\quad -\frac{1}{2}\langle l_1', m_1'\vert\sin\theta_1 e^{-i\phi_1}\vert l_1, m_1\rangle\langle l_2', m_2'\vert\sin\theta_2 e^{i\phi_2}\vert l_2, m_2\rangle.
\end{aligned} \tag{10}$$

Using results in Table 2 we can calculate the matrix element for each l_j, m_j, l_j' and m_j' $(j=1,2)$.

3. Analytical Discussions

In this section we argue analytical approximations in cases that B of the potential term $\hat{V}_B$ in (3) is large (Subsection 3.1) and small (Subsection 3.2).

3.1. Effective Hamiltonian for Large B

In this subsection we lead an effective Hamiltonian $\hat{H}_A$ for large B.

When B is large the difference between θ_k and $\theta_{k'}$, as well as the difference between ϕ_k and $\phi_{k'}$, should be small for any pair (k,k'). We, therefore, introduce the averages θ and ϕ with the deviations from them,

$$\theta \equiv \frac{1}{N_s}\sum_{k=0}^{N_s-1}\theta_k,\ \Delta\theta_k \equiv \theta_k - \theta,\ \phi \equiv \frac{1}{N_s}\sum_{k=0}^{N_s-1}\phi_k,\ \Delta\phi_k \equiv \phi_k - \phi. \tag{11}$$

Here N_s is the total number of sites on the lattice. Assuming $\vert\Delta\theta_k\vert \ll 1$ and $\vert\Delta\phi_k\vert \ll 1$ for all k, we obtain

$$\begin{aligned}\hat{V}_{kk'} &= 1-\cos\left(\theta+\Delta\theta_k\right)\cos\left(\theta+\Delta\theta_{k'}\right)\\ &\quad -\sin\left(\theta+\Delta\theta_k\right)\sin\left(\theta+\Delta\theta_{k'}\right)\cos\left(\Delta\phi_k-\Delta\phi_{k'}\right)\\ &\sim \frac{1}{2}\left\{\left(\Delta\theta_k-\Delta\theta_{k'}\right)^2+\sin^2\theta\left(\Delta\phi_k-\Delta\phi_{k'}\right)^2\right\}\\ &= \frac{1}{2}\left\{\left(\theta_k-\theta_{k'}\right)^2+\sin^2\theta\left(\phi_k-\phi_{k'}\right)^2\right\}.\end{aligned} \tag{12}$$

Then we introduce an orthogonal matrix $A=\left[a_{kj}\right]$ ($A^{-1}=A^{\mathrm{T}}$), whose elements have the following property,

$$\sum_{j=0}^{N_s-1} a_{kj}a_{k'j}=\delta_{kk'},\ \sum_{k=0}^{N_s-1} a_{kj}a_{kj'}=\delta_{jj'}. \tag{13}$$

Using this matrix A, we change the variables θ_k and ϕ_k to ξ_j and χ_j defined by

$$\xi_j\equiv\sum_{k=0}^{N_s-1} a_{kj}\theta_k,\ \chi_j\equiv\sum_{k=0}^{N_s-1} a_{kj}\phi_k. \tag{14}$$

In addition, we impose $a_{k0}=1/\sqrt{N_s}$ for all k so that $\xi_0=\sqrt{N_s}\theta$ and $\chi_0=\sqrt{N_s}\phi$. Then we see that

$$\theta_k-\theta_{k'}=\sum_{j=1}^{N_s-1}\left(a_{kj}-a_{k'j}\right)\xi_j,\ \phi_k-\phi_{k'}=\sum_{j=1}^{N_s-1}\left(a_{kj}-a_{k'j}\right)\chi_j. \tag{15}$$

Note that here we used

$$\theta_k=\sum_{j=0}^{N_s-1} a_{kj}\xi_j,\ \phi_k=\sum_{j=0}^{N_s-1} a_{kj}\chi_j. \tag{16}$$

The potential $\hat{V}_B$ is therefore approximated as

$$\begin{aligned}\hat{V}_B &\sim \frac{B}{2}\sum_{j,j'\geq 1} C\left(j,j'\right)\left\{\xi_j\xi_{j'}+\sin^2\theta\chi_j\chi_{j'}\right\},\\ C\left(j,j'\right) &\equiv \sum_{(k,k')}\left(a_{kj}-a_{k'j}\right)\left(a_{kj'}-a_{k'j'}\right).\end{aligned} \tag{17}$$

Let us consider the kinetic term $\hat{T}$ in (2) next. Our purpose is to derive the squared angular momentum for all particles in the effective Hamiltonian. Here we mention only essential parts of the derivation. A detailed discussion is given in **Appendix A1**.

Using matrix A we introduce new operators of the angular momentum,

$$\hat{L}_{\xi,\alpha,j}\equiv\sum_{k=0}^{N_s-1} a_{kj}\hat{L}_{\alpha,k}\ \left(\alpha=x,y,z\right). \tag{18}$$

Note that

$$\begin{aligned}\hat{L}_{\xi,\pm,j} &\equiv \hat{L}_{\xi,x,j}\pm i\hat{L}_{\xi,y,j}=\sum_{k=0}^{N_s-1} a_{kj}\hat{L}_{\pm,k}\\ &= \sum_{k=0}^{N_s-1} a_{kj}\mathrm{e}^{\pm i\phi_k}\left(\pm\frac{\partial}{\partial\theta_k}+i\cot\theta_k\frac{\partial}{\partial\phi_k}\right),\\ \hat{L}_{\xi,z,j} &= \sum_{k=0}^{N_s-1} a_{kj}\hat{L}_{z,k}=\sum_{k=0}^{N_s-1} a_{kj}\left(-i\frac{\partial}{\partial\phi_k}\right),\end{aligned}$$

$$\hat{L}_{\alpha,k} = \sum_{j=0}^{N_s-1} a_{kj} \hat{L}_{\xi,\alpha,j}. \tag{19}$$

Since $\left[\hat{L}_{\alpha,k}, \hat{L}_{\alpha,k'}\right] = 0$ and $\left[\hat{L}_{\xi,\alpha,j}, \hat{L}_{\xi,\alpha,j'}\right] = 0$, we find

$$\begin{aligned} \hat{T} &= \sum_{k=0}^{N_s-1} \left(\vec{\hat{L}}_k\right)^2 = \sum_{j=0}^{N_s-1} \sum_{\alpha=x,y,z} \hat{L}_{\xi,\alpha,j}^2 \\ &= \sum_{j=0}^{N_s-1} \left\{ \frac{1}{2}\left(\hat{L}_{\xi,+,j}\hat{L}_{\xi,-,j} + \hat{L}_{\xi,-,j}\hat{L}_{\xi,+,j}\right) + \hat{L}_{\xi,z,j}^2 \right\}. \end{aligned} \tag{20}$$

Then we approximate $\hat{L}_{\xi,\pm,j}$ assuming that B is large. For $j=0$ the result is, as is discussed in **Appendix A1**,

$$\hat{L}_{\xi,\pm,j=0} \sim \frac{1}{\sqrt{N_s}} \hat{L}_{A\pm},$$

$$\hat{L}_{A\pm} \equiv \mathrm{e}^{\pm i\phi} \left\{ \pm \frac{\partial}{\partial\theta} + i\cot\theta \frac{\partial}{\partial\phi} + i\csc\theta \sum_{j=1}^{N_s-1} \left(\eta_j \frac{\partial}{\partial\tilde{\xi}_j} - \tilde{\xi}_j \frac{\partial}{\partial\eta_j} \right) \right\}. \tag{21}$$

Here we have introduced new variables $\tilde{\xi}_j$ and η_j instead of ξ_j and χ_j,

$$\tilde{\xi}_j \equiv \xi_j, \ \eta_0 \equiv \chi_0, \ \eta_j \equiv \sin\theta\chi_j \quad (j \geq 1). \tag{22}$$

For $j \geq 1$ we see that

$$\hat{L}_{\xi,\pm,j} \sim \mathrm{e}^{\pm i\phi} \left\{ \pm \frac{\partial}{\partial\xi_j} + i\cot\theta \frac{\partial}{\partial\chi_j} \right\},$$

$$\frac{1}{2}\left(\hat{L}_{\xi,+,j}\hat{L}_{\xi,-,j} + \hat{L}_{\xi,-,j}\hat{L}_{\xi,+,j}\right) \sim \frac{\partial^2}{\partial\xi_j^2} + \cot^2\theta \frac{\partial^2}{\partial\chi_j^2}. \tag{23}$$

As for $\hat{L}_{\xi,z,j}$ we obtain, without any approximations,

$$\begin{aligned} \hat{L}_{\xi,z,j} &= \sum_{k=0}^{N_s-1} a_{kj} \left(-i \frac{\partial}{\partial\phi_k} \right) = -i \sum_{k=0}^{N_s-1} a_{kj} \sum_{j'=0}^{N_s-1} \frac{\partial\chi_{j'}}{\partial\phi_k} \frac{\partial}{\partial\chi_{j'}} \\ &= -i \sum_{k=0}^{N_s-1} a_{kj} \sum_{j'=0}^{N_s-1} a_{kj'} \frac{\partial}{\partial\chi_{j'}} = -i \frac{\partial}{\partial\chi_j}, \ \hat{L}_{\xi,z,j}^2 = -\frac{\partial^2}{\partial\chi_j^2}. \end{aligned} \tag{24}$$

To summarize the results, we obtain for $j=0$

$$\sum_{\alpha=x,y,z} \hat{L}_{\xi,\alpha,0}^2 \sim \frac{1}{N_s} \left\{ \frac{1}{2}\left(\hat{L}_{A+}\hat{L}_{A-} + \hat{L}_{A-}\hat{L}_{A+}\right) + \hat{L}_{\phi}^2 \right\}. \tag{25}$$

Here we used that

$$\hat{L}_{\xi,z,0} = -i\frac{\partial}{\partial\chi_0} = -i\frac{\partial}{\partial\left(\sqrt{N_s}\phi\right)} = \frac{1}{\sqrt{N_s}} \hat{L}_{\phi}, \ \hat{L}_{\phi} \equiv -i\frac{\partial}{\partial\phi}. \tag{26}$$

For $j \geq 1$, on the other hand, we find

$$\begin{aligned} &\sum_{j=1}^{N_s-1} \sum_{\alpha=x,y,z} \hat{L}_{\xi,\alpha,j}^2 \sim -\sum_{j=1}^{N_s-1} \left\{ \frac{\partial^2}{\partial\xi_j^2} + \cot^2\theta \frac{\partial^2}{\partial\chi_j^2} \right\} - \sum_{j=1}^{N_s-1} \frac{\partial^2}{\partial\chi_j^2} \\ &= -\sum_{j=1}^{N_s-1} \left\{ \frac{\partial^2}{\partial\xi_j^2} + \left(\cot^2\theta + 1\right) \frac{\partial^2}{\partial\chi_j^2} \right\} = -\sum_{j=1}^{N_s-1} \left\{ \frac{\partial^2}{\partial\tilde{\xi}_j^2} + \frac{\partial^2}{\partial\eta_j^2} \right\}. \end{aligned} \tag{27}$$

Finally we represent the effective Hamiltonian $\hat{H}_A$ using $\tilde{\xi}_j$'s and η_j's instead of ξ_j's and χ_j's, which is given by

$$\begin{aligned}\hat{H}_A = &\frac{1}{N_s}\left\{\frac{1}{2}\left(\hat{L}_{A+}\hat{L}_{A-}+\hat{L}_{A-}\hat{L}_{A+}\right)+\hat{L}_\phi^2\right\}\\ &-\sum_{j=1}^{N_s-1}\left(\frac{\partial^2}{\partial\tilde{\xi}_j^2}+\frac{\partial^2}{\partial\eta_j^2}\right)+\frac{B}{2}\sum_{j,j'\geq 1}C(j,j')\left(\tilde{\xi}_j\tilde{\xi}_{j'}+\eta_j\eta_{j'}\right).\end{aligned} \tag{28}$$

From the first term of $\hat{H}_A$ we conclude that the energy of our model contains the term of $J(J+1)/N_s$, where J is the quantum number of the angular momentum of the system with the size N_s.

It should be noted that $\hat{L}_{A\pm}$ and $\hat{L}_\phi$ are generators of SU(2) and these generators commute with $\hat{H}_A$.

$$\left[\hat{L}_{A\pm},\hat{L}_\phi\right]=\mp\hat{L}_{A\pm},\ \left[\hat{L}_{A+},\hat{L}_{A-}\right]=2\hat{L}_\phi,\ \left[\hat{L}_{A\pm},\hat{H}_A\right]=0,\ \left[\hat{L}_\phi,\hat{H}_A\right]=0. \tag{29}$$

3.2. Energy for Small *B*

In this subsection we discuss the energy when B in the potential term(3) is small.

First we consider energy for $B=0$, where no interaction exists between particles and the ground state is given by

$$\left|\Psi_0\right\rangle\equiv\prod_{j=0}^{N_s-1}\left|l_j=0,m_j=0\right\rangle. \tag{30}$$

Since the kinetic term is given by $\sum_k l_k(l_k+1)$ with the angular momentum l_k at site k, the eigen energy is given by

$$E^{(0)}=\sum_{k=0}^{N_s-1}l_k(l_k+1). \tag{31}$$

Then the lowest energy with the total angular momentum J is given by the case we have $l_k=1$ for only J sites among all N_s sites.

$$E_J^{(0)}=J\cdot 1\cdot(1+1)=2J. \tag{32}$$

Let us discuss the energy with $J=0$ by the perturbation theory for small B with the ground state $\left|\Psi_0\right\rangle$. Since the potential term contains the constant, the first order contribution is given by

$$\Delta E_0^{(1)}=\left\langle\Psi_0\right|B\sum_{(k,k')}1\left|\Psi_0\right\rangle=B\cdot\frac{N_s\cdot n_{link}}{2}. \tag{33}$$

Note that $\sum_{(k,k')}1$ equals to the total number of the links on the lattice. The second order contribution is given by

$$\begin{aligned}\Delta E_0^{(2)}=&\sum_{(k,k')}\frac{1}{E_0^{(0)}-E_2^{(0)}}\sum_{m=0,\pm1}\left|\left\langle\Psi_2(k,k',m)\right|B\hat{V}_{kk'}\left|\Psi_0\right\rangle\right|^2,\\ \left|\Psi_2(k,k',m)\right\rangle\equiv&\left|l_k=1,m_k=m\right\rangle\left|l_{k'}=1,m_{k'}=-m\right\rangle\prod_{j\neq k,k'}\left|l_j=0,m_j=0\right\rangle.\end{aligned} \tag{34}$$

The matrix element $\left\langle\Psi_2(k,k',m)\right|\hat{V}_B\left|\Psi_0\right\rangle$ is given by non-zero terms of

$$\left\langle l_k=1,m_k=m\right|\left\langle l_{k'}=1,m_{k'}=-m\right|\hat{V}_{kk'}\left|l_k=0,m_k=0\right\rangle\left|l_{k'}=0,m_{k'}=0\right\rangle.$$

From Table 2 in Section 2 we find that it is $-1/3$ for $m=0$, while it is $1/3$ for $m=\pm 1$. Therefore

$$\Delta E_0^{(2)} = -B^2 \frac{N_s \cdot n_{link}}{24}. \tag{35}$$

Thus we obtain the energy of the ground state in the second order perturbation theory including the constant contribution,

$$E_{J=0}^{(2)} = E_0^{(0)} + \Delta E_0^{(1)} + \Delta E_0^{(2)} = B \cdot \frac{N_s \cdot n_{link}}{2} - B^2 \cdot \frac{N_s \cdot n_{link}}{24}. \tag{36}$$

Now let us consider the case $J \geq 1$ with the condition that total M is equal to J. We find the degenerate states of the lowest energy $E_J^{(0)} = 2J$. Each of these J sites, say $\{i_1, i_2, \cdots, i_J\}$ sites, has the quantum number $l=1$ as well as $m=1$, while other sites have $l=0$ and $m=0$. Explicitly, this state is defined by

$$\left|\psi_{\{i_1,i_2,\cdots,i_J\}}\right\rangle \equiv \prod_{k=1,J} \left|l_{i_k}=1, m_{i_k}=1\right\rangle \prod_{j\notin\{i_1,i_2,\cdots,i_J\}} \left|l_j=0, m_j=0\right\rangle. \tag{37}$$

For small B we assume that the lowest energy state $\left|\Psi_J\right\rangle$ is totally symmetric with $\{i_1, i_2, \cdots, i_J\}$. This state is given by

$$\left|\Psi_J\right\rangle \equiv \left\{ \sum_{\{i_1,i_2,\cdots,i_J\}} \left|\psi_{\{i_1,i_2,\cdots,i_J\}}\right\rangle \right\} C, \ C \equiv \frac{1}{\sqrt{{}_{N_s}C_J}}. \tag{38}$$

Note that we have ${}_{N_s}C_J$ combinations to select sites $\{i_1, i_2, \cdots, i_J\}$. The first order energy is given by

$$\Delta E_J^{(1)} = \left\langle \Psi_J \middle| \hat{V}_B \middle| \Psi_J \right\rangle. \tag{39}$$

Since $\hat{V}_B$ has the constant term $B\sum_{(k,k')} 1$ in addition to the interactions, $\left\langle \Psi_J \middle| \hat{V}_B \middle| \Psi_J \right\rangle$ is the sum of the contributions from the diagonal elements of $\hat{V}_B$ and that of the off-diagonal elements. Namely, we denote

$$\left\langle \Psi_J \middle| \hat{V}_B \middle| \Psi_J \right\rangle = V_{diag} + V_{offd}, \ V_{diag} \equiv \left\langle \Psi_J \middle| B \sum_{(k,k')} 1 \middle| \Psi_J \right\rangle = B \cdot \frac{N_s \cdot n_{link}}{2}. \tag{40}$$

In order to obtain V_{offd} let us first calculate the matrix element $\left\langle \psi_{(i_1',i_2',\cdots,i_J')} \middle| \hat{V}_{kk'} \middle| \psi_{(i_1,i_2,\cdots,i_J)} \right\rangle$, for (k,k'), which is the pair of neighbor sites of the link, with conditions

$$i_1 = k, \ i_1' = k', \ \{i_2', i_3', \cdots, i_J'\} = \{i_2, i_3, \cdots, i_J\}. \tag{41}$$

Note that we need these conditions for the matrix element to be non-zero. Using Table 2 we obtain the matrix element

$$\begin{aligned}
&\left\langle \psi_{\{k',i_2,\cdots,i_J\}} \middle| \hat{V}_{kk'} \middle| \psi_{\{k,i_2,\cdots,i_J\}} \right\rangle \\
&= \left\langle l_k=0, m_k=0 \middle| \left\langle l_{k'}=1, m_{k'}=1 \middle| \hat{V}_{kk'} \middle| l_k=1, m_k=1 \right\rangle \middle| l_{k'}=0, m_{k'}=0 \right\rangle \\
&= -\frac{1}{2} \left\langle l_k=0, m_k=0 \middle| \sin\theta_k e^{-i\phi_k} \middle| l_k=1, m_k=1 \right\rangle \\
&\quad \times \left\langle l_{k'}=1, m_{k'}=1 \middle| \sin\theta_{k'} e^{i\phi_{k'}} \middle| l_{k'}=0, m_{k'}=0 \right\rangle \\
&= -\frac{1}{3}.
\end{aligned} \tag{42}$$

Now we need to calculate the number N_{total} which gives us the element (42) to V_{offd}. In order to derive N_{total}, first we count a number of possible cases for i_1, which is ${}_{N_s}C_1 = N_s$ clearly. Second, we count the number of possible cases for i_1'. It is ${}_{n_{link}}C_1 = n_{link}$, because the site i_1' has to be connected with the site i_1 through a link from i_1. Then we count a number of possible cases for $\{i_2, i_3, \cdots, i_J\}$. They can be putted at any site except for the two sites i_1 and i_1'. Therefore the count number is ${}_{N_s-2}C_{J-1}$. Thus the number N_{total} is given by

$$N_{total} = {}_{N_s}C_1 \cdot {}_{n_{link}}C_1 \cdot {}_{N_s-2}C_{J-1} = N_s \cdot n_{link} \cdot \frac{(N_s-2)!}{(N_s-J-1)!(J-1)!}. \tag{43}$$

We, therefore, obtain the contribution V_{offd},

$$V_{offd} \equiv N_{total} \cdot C^2\left(-\frac{B}{3}\right) = -\frac{B}{3} \cdot n_{link} J \frac{N_s - J}{N_s - 1}. \tag{44}$$

Including the contribution from the diagonal elements we obtain the energy in the first order perturbation theory,

$$E_{J\geq 1}^{(1)} = E_J^{(0)} + \Delta E_J^{(1)} = 2J + B\frac{N_s n_{link}}{2} - \frac{B}{3} n_{link} J \frac{N_s - J}{N_s - 1}. \tag{45}$$

For our model on the square lattice we fix $n_{link} = 4$.

4. Preparations for Numerical Study

4.1. Parameter $l_{\max}$

In numerical calculation we assign quantum numbers (l_k, m_k) to the state at each site *k*, where $0 \leq l_k \leq l_{\max}$ and $|m_k| \leq l_k$. The parameter $l_{\max}$ is not a physical one but should be large enough so that the energy eigen value we numerically calculate is almost irrelevant to the value of $l_{\max}$. Since total number of states amount to $\left\{(l_{max}+1)^2\right\}^{N_s}$, we need more and more computer resources for larger $l_{\max}$.

Let us numerically examine the effect of $l_{\max}$ on energy eigen values. In Table 3 and Table 4 we present the energy eigen values with several values of B on the $N_s = 5$ lattice, which are obtained by the diagonalization. The results in Table 3 (Table 4) are calculated for fixed value $M = 0$ ($M = 4$). Values of $l_{\max}$

Table 3. Energy on the $N_s = 5$ lattice for various values of B and $l_{\max}$. Here we fix $M = 0$. These results are obtained by the diagonalization.

$l_{\max}$	$B=0.5$	$B=1$	$B=2$	$B=5$	$B=10$
2	4.72835	8.64712			
3	4.72832	8.64422	14.18348		
4		8.64421	14.18118	24.73659	
5			14.18116	24.72723	36.51471
6				24.72698	36.49760
7					36.49677

Table 4. Energy on the $N_s = 5$ lattice for various values of B and $l_{\max}$. Here we fix $M = 4$. These results are obtained by the diagonalization.

$l_{\max}$	$B = 0.5$	$B = 1$	$B = 2$	$B = 5$	$B = 10$
2	11.82175				
3	11.80849	14.74603			
4	11.80843	14.74394	19.38923		
5		14.74393	19.38851	29.34678	
6			19.38851	29.34457	40.89607
7				29.34452	40.89215

are shown in the first column of these tables. Note that it is a reasonable assumption that the energy with less value of J is smaller than that with greater value of J. We therefore consider that by fixing M we can obtain the energy eigen value with $J = M$.

In Table 3 we show the lowest energies with $M = 0$ for several values of B and $l_{\max}$. There we find that the difference between the eigen values with $l_{\max} = 2$ and $l_{\max} = 3$ for $B = 0.5$ is small enough. While the results indicate that we should employ $l_{\max} = 7$ when $B = 10$. It is clear that larger value of $l_{\max}$ is necessary when B increases. We also see that values of $l_{\max}$ for $M = 4$ in Table 4 should be larger than those for $M = 0$ in Table 3.

4.2. Parameters β and l_t

For larger lattices with $N_s = 16, 36$ and 64 we calculate the energy gaps using quantum Monte Carlo methods [43] [44] [45]. In quantum Monte Carlo methods, we need two technical parameters, which are the inverse temperature β and Trotter number l_t. To calculate the lowest energy, we should employ large β as well as large l_t. Since we are interested in the energy differences, we examine how the differences depend on values of β and l_t. In Table 5 we present the energy differences on $N_s = 16$ lattice with $\beta = 12, 14.4$ and 16 and with several values of l_t between 120 and 200. Here we find the results are consistent within the statistical error. Therefore, in order to save our CPU time, we fix $\beta = 12$ and $l_t = 120$ in our Monte Carlo study. As for parameter $l_{\max}$, we employ $l_{\max} = 3$ taking account of the statistical error.

5. Numerical Study

5.1. $N_s = 2$ Case with Large B

In the previous section we present the effective Hamiltonian for large values of B with N_s sites. Here we fix $N_s = 2$ and denote the Hamiltonian by $\hat{H}_{A,2}$. From (28) in Subsection 3.1 it is given by

$$\hat{H}_{A,2} = \hat{H}_L + \hat{H}_O,$$

Table 5. Energy differences on the $N_s = 16$ lattice obtained by quantum Monte Carlo methods for various values of inverse temperature β and Trotter number l_t. Here we fix $B = 2.0$. The energy difference $\Delta E(J)$ is defined by $E(J) - E(0)$ and its error is estimated by the statistical fluctuation only.

β	l_t	$\Delta E(4)$	$\Delta E(8)$
12	120	2.12 ± 0.07	6.83 ± 0.06
12	144	2.26 ± 0.08	6.95 ± 0.08
14.4	144	2.00 ± 0.06	6.88 ± 0.07
14.4	180	2.17 ± 0.07	6.93 ± 0.07
16	160	2.04 ± 0.06	6.82 ± 0.07
16	180	2.03 ± 0.08	6.83 ± 0.06
16	200	2.06 ± 0.06	6.87 ± 0.06

$$\hat{H}_L \equiv \frac{1}{2}\left(\vec{\hat{L}}_{A,2}\right)^2 = \frac{1}{2}\left\{\frac{1}{2}\left(\hat{L}_{A+,2}\hat{L}_{A-,2} + \hat{L}_{A-,2}\hat{L}_{A+,2}\right) + \hat{L}_\phi^2\right\},$$

$$\hat{L}_{A\pm,2} \equiv \mathrm{e}^{\pm i\phi}\left\{\pm\frac{\partial}{\partial\theta} + i\cot\theta\frac{\partial}{\partial\phi} + i\csc\theta\left(\eta_1\frac{\partial}{\partial\tilde{\xi}_1} - \tilde{\xi}_1\frac{\partial}{\partial\eta_1}\right)\right\},\ \hat{L}_\phi \equiv -i\frac{\partial}{\partial\phi}$$

$$\hat{H}_O \equiv -\left(\frac{\partial^2}{\partial\tilde{\xi}_1^2} + \frac{\partial^2}{\partial\eta_1^2}\right) + 2B\left(\tilde{\xi}_1^2 + \eta_1^2\right). \tag{46}$$

When we represent $\hat{H}_{A,2}$ by variables ρ and τ, where $\tilde{\xi}_1 = \rho\cos\tau$ and $\eta_1 = \rho\sin\tau$, we have

$$\hat{L}_{A\pm,2} \equiv \mathrm{e}^{\pm i\phi}\left(\pm\frac{\partial}{\partial\theta} - \cot\theta\hat{L}_\phi - \csc\theta\hat{L}_\tau\right),\ \hat{L}_\tau \equiv -i\frac{\partial}{\partial\tau},$$

$$\hat{H}_L = \frac{1}{2}\left\{-\frac{\partial^2}{\partial\theta^2} - \cot\theta\frac{\partial}{\partial\theta} - \csc^2\theta\left(\frac{\partial^2}{\partial\phi^2} + \frac{\partial^2}{\partial\tau^2} + 2\cos\theta\frac{\partial^2}{\partial\phi\partial\tau}\right)\right\},$$

$$\hat{H}_O = -\left(\frac{\partial^2}{\partial\rho^2} + \frac{1}{\rho}\frac{\partial}{\partial\rho} + \frac{1}{\rho^2}\frac{\partial^2}{\partial\tau^2}\right) + 2B\rho^2. \tag{47}$$

Since the eigen values of $\hat{H}_L$ and $\hat{H}_O$ in (47) are well known, we see the eigen energy of $\hat{H}_{A,2}$ is given by

$$E_{A,2}(J, M, n_\rho, m_\tau) = \frac{1}{2}J(J+1) + 2\sqrt{2B}(1+n_\rho),$$

$$n_\rho = 0,1,2,\cdots,\ m_\tau = -n_\rho, -n_\rho+2, \cdots, n_\rho-2, n_\rho,$$

$$J = |m_\tau|, |m_\tau|+1, |m_\tau|+2, \cdots,\ M = -J, -J+1, \cdots, 0, \cdots, J-1, J. \tag{48}$$

Note that $n_\rho = n_{\tilde{\xi}_1} + n_{\eta_1}$ with $n_{\tilde{\xi}_1}, n_{\eta_1} = 0,1,2,\cdots$, $m_\tau = n_{\tilde{\xi}_1} - n_{\eta_1} = n_\rho - 2n_{\eta_1} = 2n_{\tilde{\xi}_1} - n_\rho$ and therefore $\Delta m_\tau = 2$. The condition of $J \geq |m_\tau|$ in (48) is non-trivial. The reason for this condition is described in **Appendix A2**.

In order to confirm the eigen values in (48) we carry out numerical calcula-

tions of the system with two particles. We employ the diagonalization to obtain all energy values when $l_{\max}=7$. The results are shown in Figure 1 ($B=18$) and Figure 2 ($B=50$). The lower (upper) line in the figures plots $E_{A,2}$ for $n_\rho=0(1)$. From these figures we find that the $E_{A,2}$ describes the numerical results well, especially for $B=50$ found in Figure 2. In addition, by the extensive calculations, we successfully observe the excited energy near the upper lines. Here we should note two features. The first one is that the lowest value of J is 1 for $n_\rho=1$. The reason is as follows. When $n_\rho=1$ ($n_{\tilde{\xi}_1}=1$ and $n_{\eta_1}=0$ or $n_{\tilde{\xi}_1}=0$ and $n_{\eta_1}=1$), which means we have the excited state of $\tilde{\xi}_1$ or η_1, we obtain $m_\tau=1$ or $m_\tau=-1$. Because of the condition $J\geq|m_\tau|$ in (48) J should be greater than or equal to 1. The second feature is that the two states near the upper lines are almost degenerate. We hardly can distinguish the state of $m_\tau=1$ from that of $m_\tau=-1$, especially for $B=50$.

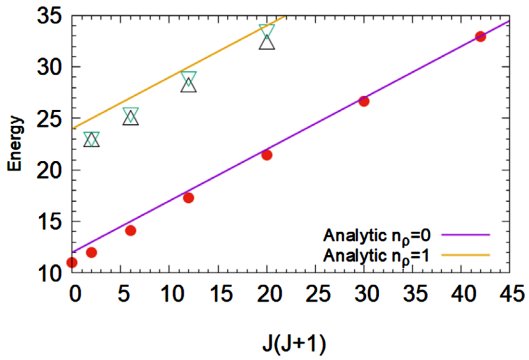

Figure 1. Energy versus $J(J+1)$ for $B=18$ and $N_s=2$. Energies obtained by the diagonalization are plotted by filled red circles and blue and green triangles. Analytic results $J(J+1)/2+2\sqrt{2B}(n_\rho+1)$ are represented by the violet line ($n_\rho=0$) and the orange line ($n_\rho=1$). It should be noted that blue and green triangles are close to each others.

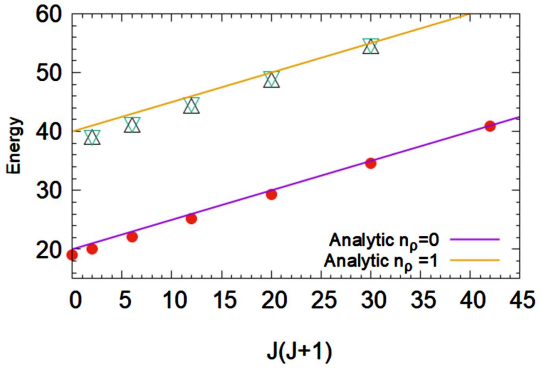

Figure 2. Energy versus $J(J+1)$ for $B=50$ and $N_s=2$. Energies obtained by the diagonalization are plotted by filled red circles and blue and green triangles. Analytic results $J(J+1)/2+2\sqrt{2B}(n_\rho+1)$ are represented by the violet line ($n_\rho=0$) and the orange line ($n_\rho=1$). It should be noted that blue and green triangles are close to each others.

These results strongly support our theoretical arguments on the effective Hamiltonian $\hat{H}_L$ in (47) which includes the additional terms of $\partial/\partial\tau$.

5.2. Larger Lattices

For the numerical study on $N_s = 8$ lattice, we apply stochastic state selection (SSS) method, which is easy to implement and reliable. We find that $l_{\max} = 4$ is enough to keep the precision of SSS method. For the lattices with $N_s = 16, 36$ and 64 we use quantum Monte Carlo methods with $\beta = 12$, $l_t = 120$ and $l_{\max} = 3$.

Let us first calculate the energy eigen values for small value of *B*. In Subsection 3.2 we made theoretical study for this case, where we found that the energy differences are described by the liner function of *J*. Figure 3 shows our numerical results for $B = 0.3$ and $N_s = 8, 16, 36$ and 64 as a function of *J*. Solid lines in the figure are obtained by the least square fit. We find that all data of each lattice shows good linearity and the slopes show little dependency on the lattice size. In the perturbation theory in Subsection 3.2, the energy $E^{(1)}_{J\geq 1}$ in (45) for large N_s linearly depends on *J* and the slopes of the lines are $2 - 4B/3$ at the first order of *B*. When $B = 0.3$ this slope is 1.6, which should be compared with the numerical result 1.75 ± 0.01. We therefore conclude that for $B < 0.3$ our model is in a phase where the energy linearly increases as *J* becomes large. We see that in this region of small *B* the gap energy is constant even if the lattice size is large, so we call this phase "gaped energy state (GES) phase".

Next we present our results for large *B*, which would be given by a linear function of $J(J+1)$ derived from the Hamiltonian $\hat{H}_A$ (28) in Subsection 3.1. We show the energy for $B = 2.0$ in Figure 4 as a function of $J(J+1)$, together with solid lines obtained by the least square fit. We find good linearity for

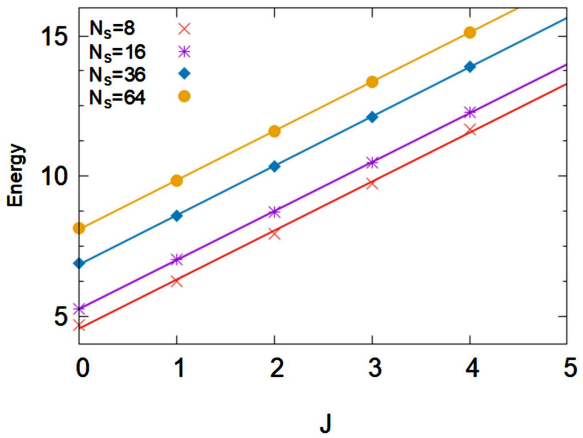

Figure 3. Energy with $B = 0.3$ plotted as a function of *J*. The red crosses, the violet asterisks, the blue diamonds and the orange circles are results for $N_s = 8, 16, 36$ and 64, respectively. The data for $N_s = 8$ are obtained by SSS method, while others are by quantum Monte Carlo methods. In the figure we plot $(E_J - C_{N_s})$, where $C_8 = 0$, $C_{16} = 4$, $C_{36} = 14$ and $C_{64} = 29$, so that we can see the data easily. The error of the data is smaller than the magnitude of the symbol. The solid lines are obtained by the least square fit.

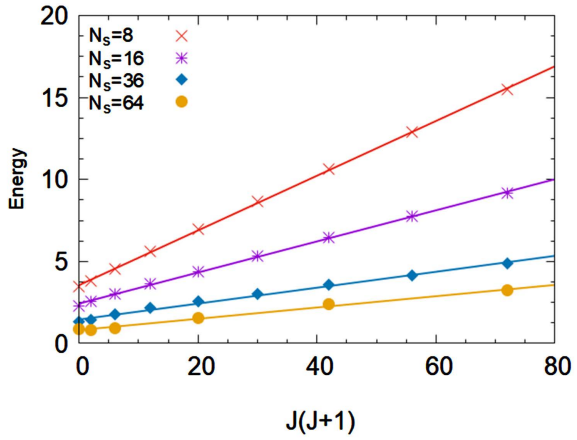

Figure 4. Energy with $B=2.0$ plotted as a function of $J(J+1)$. The red crosses, the violet asterisks, the blue diamonds and the orange circles are results for $N_s=8,16,36$ and 64, respectively. The data for $N_s=8$ are obtained by SSS method, while others are by quantum Monte Carlo methods. In the figure we plot $(E_J-C_{N_s})$, where $C_8=20$, $C_{16}=44$, $C_{36}=104$ and $C_{64}=187$, so that we can see the data easily. The error of the data is smaller than the magnitude of the symbol. The solid lines are obtained by the least square fit.

any lattice size, which holds even for $B=2.0$. Our argument in Subsection 3.1 leads us that the slope should be $1/N_s$ for quite large B. When the slopes in **Figure 4** is fitted to $c(B,N_s)/N_s$, values of $c(B,N_s)$ distribute from 1.5 to 2.0 for $N_s=8,16,36$ and 64.

Now we will numerically confirm that the energy differences are described by $J(J+1)/N_s$ for quite large B. We carry out our calculations on $N_s=5$ lattice since we have to employ large value of $l_{\max}$, which we fix $l_{\max}=7$ according to results in **Table 3** and **Table 4**. Using the diagonalization we find $c(B,N_s=5)=1.302,1.154,1.100$ and 1.067 for $B=2,5,10$ and 20, respectively. These results indicate that $c(B,N_s)$ becomes 1 when B is quite large, which strongly supports our theoretical arguments in Subsection 3.1. In the region of large B the gap energy decreases when the lattice size becomes large. We therefore conclude that the system is in "SSB phase" since there exist QDS, which is a characteristic feature of SSB.

From our results we see at least two different phases, GES phase with small B and SSB phase with large B. In **Figure 5** ($N_s=8,16$) and **Figure 6** ($N_s=36,64$) we show the differences between the obtained results and values given by the fitted lines using D_1 and D_2, whose definitions are

$$D_1 \equiv \frac{1}{n_{data}}\sum_J \{E_J - a_1 J - b_1\}^2,$$

$$D_2 \equiv \frac{1}{n_{data}}\sum_J \{E_J - a_2 J(J+1) - b_2\}^2. \tag{49}$$

Here n_{data} is a number of the calculated energy E_J. $a_1(a_2)$ and $b_1(b_2)$ of the fitted lines are numerically determined imposing $D_1(D_2)$ should be minimum.

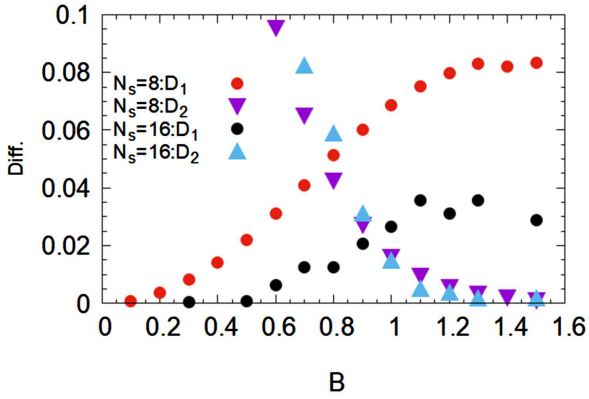

Figure 5. D_1 and D_2 defined by (49) as a function of B. The red circles (the violet triangles) plot D_1 (D_2) for $N_s = 8$, while the black circles (the blue triangles) plot D_1 (D_2) for $N_s = 16$. We employ the data with $J = 0,1,2,3$ and 4 to calculate them.

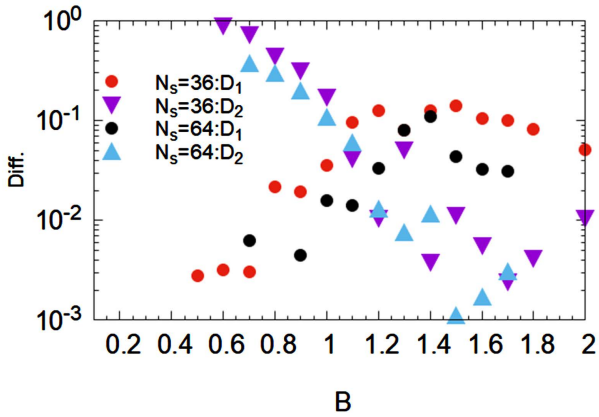

Figure 6. D_1 and D_2 defined by (49) as a function of B. The red circles (the violet triangles) plot D_1 (D_2) for $N_s = 36$, while the black circles (the blue triangles) plot D_1 (D_2) for $N_s = 64$. We employ the data with $J = 0,2,4,6$ and 8 ($J = 2,4,6,8$ and 10) for $N_s = 36$ (64) to calculate them.

In these figures we find that D_1 increases when B becomes large, while D_2 decreases. We see that D_1 is smaller than D_2 for $N_s = 8$ when $B < 0.8$, while $D_1 \sim D_2$ at $B = 0.8$. The value of B where D_1 is comparable with D_2 depends on the lattice size, which are roughly 0.8, 0.9, 1.1 and 1.15 for $N_s = 8,16,36$ and 64. These results indicate that the value of B where $D_1 \sim D_2$ is observed to increase slightly when the lattice becomes large.

6. Summary and Discussion

What we are interested in is to observe the violation of the cluster property [16] [17], when the continuous symmetry in the system breaks spontaneously. In recent work [31] we examined the nonlinear sigma model with U(1) symmetry. Then we came to a conclusion that there exist QDS, the quasi-degenerate states, whose energies are dependent on the quantum number of the angular momentum and the system size.

In the present work we studied the nonlinear sigma model with SU(2) symmetry. This model is more interesting than the one with U(1) symmetry because of deep connection with Heisenberg spin model. Using the improved technique, we examined to see if the model has QDS. We considered the quantum model defined on the square lattice and employed the representation where the kinetic term is diagonalized, so that we can carry out numerical calculations with the fixed quantum numbers.

Before studying the model numerically we made analytical discussions for large B and for small B, where B is the strength of the potential term. In the region of large B we found that the energy gap is proportional to $J(J+1)/N_s$, where N_s denotes the system size and the quantum number J is the total angular momentum for the system. We, therefore, see this gap becomes 0 in the limit $N_s \to \infty$. Since this result means that there exist QDS, which is a characteristic feature of SSB, we called this phase "spontaneous symmetry breaking (SSB) phase". When B is small, on the other hand, we found that the energy gap hardly depends on N_s. We therefore call this phase "gaped energy state (GES) phase". In this phase we also derived that the energy gap is proportional to J.

Our numerical results in Section 5, which we have obtained by the diagonalization on the $N_s = 2$ lattice, by stochastic state selection method [35]-[42] on the $N_s = 8$ lattice and by quantum Monte Carlo methods on the $N_s = 16, 36$ and 64 lattices, strongly support that the model has these two phases.

Finally two comments are added. The first comment is on the study of the phase transition between GES phase and SSB phase. Many researchers have discussed the scaling behavior of the susceptibility and others at the critical point using the renormalization group method [6] [7] [47]. We notify that our Hamiltonian and our numerical approach would be quite useful for these studies. In the present work about the two-dimensional nonlinear sigma model, we have observed that the system is in GES phase when the interaction is weak, while it is in SSB phase with the strong interaction. We expect that our approach will also be prosperous in investigations of the one-dimensional nonlinear sigma model, which is intriguing in research of the field theory [48].

The second comment is on representations of SU(2). In our present study for large B we derived operators $\hat{L}_{A\pm}$ of the angular momentum, which includes an additional term in comparison with the conventional one. This term is well known in fields of mathematical physics, where relations between the generalized SU(2) algebra and the special functions [46] [49] [50] were studied. Our $\hat{L}_{A\pm}$ and $\hat{L}_{\phi}$ operators show the generalized algebra, which is called the spin-weighed harmonics. In investigations of gravity, monopole and so on we can find many works on this algebra. In the study of gravity this algebra was first derived 50 years ago [51], while we can also find this algebra in a recent work [52]. In the study of the monopole, this algebra has been first proposed in [53] and further studies in [54] [55] have made it clear that the Hamiltonian with the potential due to the monopole has the spin-weighed harmonics. We see that our Hamiltonian for large B is another example for this algebra. We therefore think

that this Hamiltonian should be studied more extensively from algebraic point of view.

Conflicts of Interest

The authors declare no conflicts of interest regarding the publication of this paper.

Acknowledgements

I sincerely thank Dr. Yasuko Munehisa, who made the valuable comments on the manuscript. Especially the discussion on Section 3 was made clear by her suggestion.

References

[1] Auerbach, A. (1994) Interacting Electrons and Quantum Magnetism. Springer-Verlag, Berlin, Heidelberg. https://doi.org/10.1007/978-1-4612-0869-3

[2] Chen, Y. and Castro Neto, A.H. (2000) Effective Field Theory for Layered Quantum Antiferromagnets with Nonmagnetic Impurities. *Physics Review B*, **61**, R3772-R3775. https://doi.org/10.1103/PhysRevB.61.R3772

[3] Dupré, T. (1996) Localization Transition in Three Dimensions: Monte Carlo Simulation of Nonlinear σ Model. *Physics Review B*, **54**, 12763-12774. https://doi.org/10.1103/PhysRevB.54.12763

[4] Schaefer, L. and Wegner, F. (1980) Disordered System with n Orbitals per Site: Lagrange Formulation, Hyperbolic Symmetry, and Goldstone Modes. *Zeitschrift Für Physik B Condensed Matter*, **38**, 113-126. https://doi.org/10.1007/BF01598751

[5] Haldane, F. (1983) Nonlinear Field Theory of Large-Spin Heisenberg Antiferromagnets: Semiclassically Quantized Solitons of the One-Dimensional Easy-Axis Néel State. *Physical Review Letters*, **50**, 1153-1156. https://doi.org/10.1103/PhysRevLett.50.1153

[6] Chakravarty, S., Halperin, B. and Nelson, D.R. (1989) Two-Dimensional Quantum Heisenberg Antiferromagnet at Low Temperatures. *Physics Review B*, **39**, 2344-2371. https://doi.org/10.1103/PhysRevB.39.2344

[7] Chubukov, A., Sachdev, S. and Ye, J. (1994) Theory of Two-Dimensional Quantum Heisenberg Antiferromagnets with a Nearly Critical Ground State. *Physics Review B*, **49**, 11919-11961. https://doi.org/10.1103/PhysRevB.49.11919

[8] Bulgadaev, S. (2000) D-Dimensional Confromal Sigma-Models and Their Topological Excitation. arXiv:hep-th/0008017

[9] Alles, B., Borisenko, O. and Papa, A. (2018) Finite Density 2D O(3) Sigma Model: Dualization and Numerical Simulations. *Physics Review D*, **98**, Article ID: 114508. https://doi.org/10.1103/PhysRevD.98.114508

[10] Abanov, A. and Wiegmann, P. (2000) Chiral Non-Linear Sigma-Models as Models for Topological Superconductivity. *Physical Review Letters*, **86**, 1319.

[11] Scherer, S. (2002) Introduction to Chiral Perturbation Theory. arXiv:hep-ph/0210398.

[12] da Costa, R. (1981) Quantum Mechanics of a Constrained Particle. *Physical Review A*, **23**, 1982-1987. https://doi.org/10.1103/PhysRevA.23.1982

[13] da Silva, L., Bastos, C. and Ribeiro, F. (2017) Quantum Mechanics of a Constrained

Particle and the Problem of Prescribed Geometry-Induced Potential. *Annals of Physics*, **379**, 13-33. https://doi.org/10.1016/j.aop.2017.02.012

[14] Dandoloff, R., Jensen, B. and Saxena, A. (2014) Generalized Anti-Centrifugal Potential. *Physics Letters A*, **378**, 510-513. https://doi.org/10.1016/j.physleta.2013.12.016

[15] Dandoloff, R. (2019) Topologically Stable States of the Anti-Centrifugal Potential. *Journal of Modern Physics*, **10**, 1002-1005. https://doi.org/10.4236/jmp.2019.108066

[16] Weinberg, S. (1995) The Quantum Theory of Fields. Vol. 2, Cambridge University Press, Cambridge.

[17] Strocchi, F. (2008) Symmetry Breaking. In: *Lecture Note Physics*, Vol. 732, Springer, Berlin. https://doi.org/10.1007/978-3-540-73593-9

[18] Munehisa, T. (2018) Violation of Cluster Property in Quantum Antiferromagnet. *World Journal of Condensed Matter Physics*, **8**, 1-22. https://doi.org/10.4236/wjcmp.2018.81001

[19] Munehisa, T. (2018) Violation of Cluster Property in Heisenberg Antiferromagnet. *World Journal of Condensed Matter Physics*, **8**, 203-229. https://doi.org/10.4236/wjcmp.2018.84015

[20] Munehisa, T. (2020) Quantum Curie-Weiss Magnet Induced by Violation of Cluster Property. *World Journal of Condensed Matter Physics*, **10**, 27-52. https://doi.org/10.4236/wjcmp.2020.102003

[21] Richter, J., Schulenburg, J. and Honecker, A. (2004) Quantum Magnetism. In: Schollwock, U., Richter, J., Farnell, D.J.J. and Bishop, R.F., Eds., *Lecture Note in Physics*, Vol. 645, Springer-Verlag, Berlin Heidelberg, 85-153. https://doi.org/10.1007/BFb0119592

[22] Manousakis, E. (1991) The Spin-½ Heisenberg Antiferromagnet on a Square Lattice and Its Application to the Cuprous Oxides. *Review Modern of Physics*, **63**, 1-62. https://doi.org/10.1103/RevModPhys.63.1

[23] Landee, C. and Turnbull, M. (2013) Recent Developments in Low-Dimensional Copper (II) Molecular Magnets. *European Journal of Inorganic Chemistry*, **2013**, 2250. https://doi.org/10.1002/ejic.201300268

[24] Dell'Anna, L., Salberger, O., Barbiero, L., Trombettoni, A. and Korepin, V. (2016) Violation of Cluster Decomposition and Absence of Light Cones in Local Integer and Half-Integer Spin Chains. *Physics Review B*, **94**, Article ID: 155140. https://doi.org/10.1103/PhysRevB.94.155140

[25] Shimizu, A. and Miyadera, T. (2002) Cluster Property and Robustness of Ground States of Interacting Many Bosons. *Journal of the Physical Society of Japan*, **71**, 56-59. https://doi.org/10.1143/JPSJ.71.56

[26] Shimizu, A. and Miyadera, T. (2002) Stability of Quantum States of Finite Macroscopic Systems against Classical Noises, Perturbations from Environments, and Local Measurements. *Physical Review Letters*, **89**, Article ID: 270403. https://doi.org/10.1103/PhysRevLett.89.270403

[27] Xu, S. and Fan, S. (2017) Generalized Cluster Decomposition Principle Illustrated In Waveguide Quantum Electrodynamics. *Physics Review A*, **95**, Article ID: 063809. https://doi.org/10.1103/PhysRevA.95.063809

[28] Fröhlich, J. and Rodríguez P. (2017) On Cluster Properties of Classical Ferromagnets in an External Magnetic Field. *Journal of Statistical Physics*, **166**, 828-840. https://doi.org/10.1007/s10955-016-1556-2

[29] Strocchi, F. (1978) Local and Covariant Gauge Quantum Field Theories. Cluster

Property, Superselection Rules, and the Infrared Problem. *Physics Review D*, **17**, 2010-2021. https://doi.org/10.1103/PhysRevD.17.2010

[30] Lowdon, P. (2016) Conditions on the Violation of the Cluster Decomposition Property in QCD. *Journal of Mathematical Physics*, **57**, Article ID: 102302. https://doi.org/10.1063/1.4965715

[31] Munehisa, T. (2021) Degenerate States in Nonlinear Sigma Model with U(1) Symmetry—For Study on Violation of Cluster Property. *World Journal of Condensed Matter Physics*, **11**, 29-52. https://doi.org/10.4236/wjcmp.2021.113003

[32] Schmüdgen, K. (1983) On the Heisenberg Commutation Relation. I. *Journal of Functional Analysis*, **50**, 8-49. https://doi.org/10.1016/0022-1236(83)90058-7

[33] Albeverio, S. and Sengupta, A. (2016) Complex Phase Space and Weyl's Commutation Relations. *Expositiones Mathematicae*, **34**, 249-286. https://doi.org/10.1016/j.exmath.2015.12.006

[34] Arai, A. (2016) A Family of Inequivalent Weyl Representations of Canonical Commutation Relations with Applications to Quantum Field Theory. *Reviews in Mathematical Physics*, **28**, Article 1650007. https://doi.org/10.1142/S0129055X16500070

[35] Munehisa, T. and Munehisa, Y. (2003) A New Approach to Stochastic State Selections in Quantum Spin Systems. *Journal of the Physical Society of Japan*, **72**, 2759-2765. https://doi.org/10.1143/JPSJ.72.2759

[36] Munehisa, T. and Munehisa, Y. (2004) The Stochastic State Selection Method for Energy Eigenvalues in the Shastry-Sutherland Model. *Journal of the Physical Society of Japan*, **73**, 340-347. https://doi.org/10.1143/JPSJ.73.340

[37] Munehisa, T. and Munehisa, Y. (2004) Numerical Study for an Equilibrium in the Recursive Stochastic State Selection Method. arXiv:cond-mat/0403626

[38] Munehisa, T. and Munehisa, Y. (2004) A Recursive Method of the Stochastic State Selection for Quantum Spin Systems. *Journal of the Physical Society of Japan*, **73**, 2245-2251. https://doi.org/10.1143/JPSJ.73.2245

[39] Munehisa, T. and Munehisa, Y. (2006) The Stochastic State Selection Method Combined with the Lanczos Approach to Eigenvalues in Quantum Spin Systems. *Journal of Physics*: *Condensed Matter*, **18**, 2327-2335. https://doi.org/10.1088/0953-8984/18/7/018

[40] Munehisa, T. and Munehisa, Y. (2007) An Equilibrium for Frustrated Quantum Spin Systems in the Stochastic State Selection Method. *Journal of Physics*: *Condensed Matter*, **19**, 196202. https://doi.org/10.1088/0953-8984/19/19/196202

[41] Munehisa, T. and Munehisa, Y. (2009) A Constrained Stochastic State Selection Method Applied to Frustrated Quantum Spin Systems. *Journal of Physics*: *Condensed Matter*, **21**, 236008. https://doi.org/10.1088/0953-8984/21/23/236008

[42] Munehisa, T. and Munehisa, Y. (2010) Numerical Study of the Spin-1/2 Heisenberg Antiferromagnet on a 48-Site Triangular Lattice Using the Stochastic State Selection Method. arXiv:1008.1612

[43] Hatano, N. and Suzuki, M. (1993) Quantum Monte Carlo Methods in Condensed Matter Physics. World Scientific, Singapore, 13-47. https://doi.org/10.1142/9789814503815_0002

[44] De Raedt, H. and von der Linden, W. (1995) The Monte Carlo Method in Condensed Matter Physics. Springer-Verlag, Berlin, Heidelberg, 249-284.

[45] Kawashima, N. (2002) Quantum Monte Carlo Methods. *Progress of Theoretical Physics Supplement*, **145**, 138-149. https://doi.org/10.1143/PTPS.145.138

[46] del Castillo, T. (2007) Spin-Weighted Spherical Harmonics and Their Applications. *Revista Mexicana de Fisica S*, **53**, 125-134.

[47] Podolsky, D. and Sachdev, S. (2012) Spectral Functions of the Higgs Mode Near Two-Dimensional Quantum Critical Points. *Physics Review B*, **86**, 054508. https://doi.org/10.1103/PhysRevB.86.054508

[48] Bruckmann, F., Jansen, K. and Kühn, S. (2019) O(3) Nonlinear Sigma Model in 1 + 1 Dimensions with Matrix Product States. *Physics Review D*, **99**, Article ID: 074501. https://doi.org/10.1103/PhysRevD.99.074501

[49] Miller, Jr. W. (1968) Lie Theory and Special Functions. Academic Press, New York.

[50] Wasson, R.D. (2013) An Overview of the Relationship between Group Theory and Representation to the Special Functions in Mathematical Physics. arXiv:1309.2544

[51] Newman, E.T. and Penrose, R. (1966) Note on the Bondi-Metzner-Sachs Group. *Journal of Mathematical Physics*, **7**, 863-870. https://doi.org/10.1063/1.1931221

[52] Boyle, M. (2016) How Should Spin-Weighted Spherical Functions Be Defined? arXiv:1604.08140

[53] Wu, T.T. and Yang, C.N. (1976) Dirac Monopole without Strings: Monopole Harmonics. *Nuclear Physics B*, **107**, 365-380. https://doi.org/10.1016/0550-3213(76)90143-7

[54] Dray, T. (1985) The Relationship between Monopole Harmonics and Spin-Weighted Spherical Harmonics. *Journal of Mathematical Physics*, **26**, 1030-1033. https://doi.org/10.1063/1.526533

[55] Prieto, C.T. (2001) Quantization and Spectral Geometry of a Rigid Body in a Magnetic Monopole Field. *Differential Geometry and Its Applications*, **14**, 157-179. https://doi.org/10.1016/S0926-2245(00)00044-9

Appendix

A1. Derivation of the Effective Kinetic Term for Large B

In Subsection 3.1 we defined θ, $\Delta\theta_k$, ϕ and $\Delta\phi_k$. We also defined $\hat{L}_{\xi,\pm,j}$ using $\hat{L}_{\pm k}$ and the orthogonal matrix $A=\left[a_{kj}\right]$ as well. In this subsection of Appendix we derive effective $\hat{L}_{\xi,\pm,j}$ presented in (21) and (23).

First note that we have the following relations from the Equation (16) for the differential operators,

$$\frac{\partial}{\partial\xi_j}=\sum_{k=0}^{N_s-1}\frac{\partial\theta_k}{\partial\xi_j}\frac{\partial}{\partial\theta_k}=\sum_{k=0}^{N_s-1}a_{kj}\frac{\partial}{\partial\theta_k},\quad \frac{\partial}{\partial\chi_j}=\sum_{k=0}^{N_s-1}\frac{\partial\phi_k}{\partial\chi_j}\frac{\partial}{\partial\phi_k}=\sum_{k=0}^{N_s-1}a_{kj}\frac{\partial}{\partial\phi_k}. \tag{50}$$

For later use we also need the following relations,

$$\begin{gathered}
\frac{\partial}{\partial\theta_k}=\sum_{j=0}^{N_s-1}a_{kj}\frac{\partial}{\partial\xi_j},\quad \frac{\partial}{\partial\phi_k}=\sum_{j=0}^{N_s-1}a_{kj}\frac{\partial}{\partial\chi_j},\\
\sum_{k=0}^{N_s-1}\phi_k\frac{\partial}{\partial\theta_k}=\sum_{k=0}^{N_s-1}\sum_{j,j'=0}^{N_s-1}a_{kj}a_{kj'}\chi_j\frac{\partial}{\partial\xi_{j'}}=\sum_{j=0}^{N_s-1}\chi_j\frac{\partial}{\partial\xi_j},\\
\sum_{k=0}^{N_s-1}\theta_k\frac{\partial}{\partial\phi_k}=\sum_{k=0}^{N_s-1}\sum_{j,j'=0}^{N_s-1}a_{kj}a_{kj'}\xi_j\frac{\partial}{\partial\chi_{j'}}=\sum_{j=0}^{N_s-1}\xi_j\frac{\partial}{\partial\chi_j},\\
\sum_{k=0}^{N_s-1}\phi_k\frac{\partial}{\partial\phi_k}=\sum_{k=0}^{N_s-1}\sum_{j,j'=0}^{N_s-1}a_{kj}a_{kj'}\chi_j\frac{\partial}{\partial\chi_{j'}}=\sum_{j=0}^{N_s-1}\chi_j\frac{\partial}{\partial\chi_j},\\
\phi\sum_{k=0}^{N_s-1}\frac{\partial}{\partial\theta_k}=\phi\sqrt{N_s}\sum_{k=0}^{N_s-1}a_{k0}\frac{\partial}{\partial\theta_k}=\chi_0\frac{\partial}{\partial\xi_0},\\
\theta\sum_{k=0}^{N_s-1}\frac{\partial}{\partial\phi_k}=\theta\sqrt{N_s}\sum_{k=0}^{N_s-1}a_{k0}\frac{\partial}{\partial\phi_k}=\xi_0\frac{\partial}{\partial\chi_0}.
\end{gathered} \tag{51}$$

We will approximate $\hat{L}_{\xi,\pm,j}$ under the conditions $\left|\Delta\theta_k\right|\ll 1$ and $\left|\Delta\phi_k\right|\ll 1$. We expand

$$\begin{gathered}
\mathrm{e}^{\pm i\phi_k}=\mathrm{e}^{\pm i\phi\pm i(\Delta\phi_k)}\sim\mathrm{e}^{\pm i\phi}\left\{1\pm i\left(\Delta\phi_k\right)\right\},\\
\cot\theta_k=\cot\left\{\theta+\left(\Delta\theta_k\right)\right\}\sim\cot\theta-\csc^2\theta\left(\Delta\theta_k\right).
\end{gathered} \tag{52}$$

Then we obtain

$$\begin{aligned}
\hat{L}_{\xi,\pm,j}&=\sum_{k=0}^{N_s-1}a_{kj}\hat{L}_{\pm k}=\sum_{k=0}^{N_s-1}a_{kj}\mathrm{e}^{\pm i\phi_k}\left(\pm\frac{\partial}{\partial\theta_k}+i\cot\theta_k\frac{\partial}{\partial\phi_k}\right)\\
&\sim\sum_{k=0}^{N_s-1}a_{kj}\mathrm{e}^{\pm i\phi}\left\{1\pm i\Delta\phi_k\right\}\left(\pm\frac{\partial}{\partial\theta_k}+i\left\{\cot\theta-\csc^2\theta\left(\Delta\theta_k\right)\right\}\frac{\partial}{\partial\phi_k}\right)\\
&\sim Z_{\pm,j}+Q_{\pm,j}+R_{\pm,j}+S_{\pm,j},
\end{aligned}$$

$$Z_{\pm,j}\equiv\sum_{k=0}^{N_s-1}a_{kj}\mathrm{e}^{\pm i\phi}\left(\pm\frac{\partial}{\partial\theta_k}+i\cot\theta\frac{\partial}{\partial\phi_k}\right),$$

$$Q_{\pm,j}\equiv\sum_{k=0}^{N_s-1}a_{kj}\mathrm{e}^{\pm i\phi}\left(\pm i\right)\left(\Delta\phi_k\right)\left(\pm\frac{\partial}{\partial\theta_k}\right),$$

$$R_{\pm,j} \equiv \sum_{k=0}^{N_s-1} a_{kj} \mathrm{e}^{\pm i\phi} (-i) \csc^2\theta (\Delta\theta_k) \frac{\partial}{\partial \phi_k},$$

$$S_{\pm,j} \equiv \sum_{k=0}^{N_s-1} a_{kj} \mathrm{e}^{\pm i\phi} (\pm i) (\Delta\phi_k) i \cot\theta \frac{\partial}{\partial \phi_k}. \tag{53}$$

Because of (51) we find the first term becomes

$$Z_{\pm,j} = \mathrm{e}^{\pm i\phi} \left(\pm \frac{\partial}{\partial \xi_j} + i \cot\theta \frac{\partial}{\partial \chi_j} \right). \tag{54}$$

For $j \geq 1$ terms $Q_{\pm,j}$, $R_{\pm,j}$ and $S_{\pm,j}$ are negligible compared to $Z_{\pm,j}$, while $Q_{\pm,0}$, $R_{\pm,0}$ and $S_{\pm,0}$ are comparable with $Z_{\pm,0}$. The reason is as follows. When $|\Delta\theta_k| \sim O(\Delta)$ and $|\Delta\phi_k| \sim O(\Delta)$ with $\Delta \ll 1$, we also see that

$$|\xi_0| \sim O(1),\ |\chi_0| \sim O(1),\ \frac{\partial}{\partial \xi_0} \sim O(1),\ \frac{\partial}{\partial \chi_0} \sim O(1)$$

$$|\xi_j| \sim O(\Delta),\ |\chi_j| \sim O(\Delta),\ \frac{\partial}{\partial \xi_j} \sim O\left(\frac{1}{\Delta}\right),\ \frac{\partial}{\partial \chi_j} \sim O\left(\frac{1}{\Delta}\right)\ (j \geq 1). \tag{55}$$

From these estimations we find

$$|Z_{\pm,0}| \sim O(1),\ |Q_{\pm,0}| \sim O(1),\ |R_{\pm,0}| \sim O(1),\ |S_{\pm,0}| \sim O(1),$$

$$|Z_{\pm,j}| \sim O\left(\frac{1}{\Delta}\right),\ |Q_{\pm,j}| \sim O(1),\ |R_{\pm,j}| \sim O(1),\ |S_{\pm,j}| \sim O(1)\ (j \geq 1). \tag{56}$$

Let us calculate $Q_{\pm,0}$, $R_{\pm,0}$ and $S_{\pm,0}$ then. Using (51) we obtain

$$\begin{aligned} Q_{\pm,0} &= \frac{1}{\sqrt{N_s}} \mathrm{e}^{\pm i\phi} (\pm i)(\pm) \left\{ \sum_{l=0}^{N_s-1} \chi_l \frac{\partial}{\partial \xi_l} - \chi_0 \frac{\partial}{\partial \xi_0} \right\} \\ &= \frac{i}{\sqrt{N_s}} \mathrm{e}^{\pm i\phi} \sum_{l=1}^{N_s-1} \chi_l \frac{\partial}{\partial \xi_l}, \end{aligned}$$

$$\begin{aligned} R_{\pm,0} &= \frac{1}{\sqrt{N_s}} \mathrm{e}^{\pm i\phi} (-i) \csc^2\theta \left\{ \sum_{l=0}^{N_s-1} \xi_l \frac{\partial}{\partial \chi_l} - \xi_0 \frac{\partial}{\partial \chi_0} \right\} \\ &= -\frac{i}{\sqrt{N_s}} \mathrm{e}^{\pm i\phi} \csc^2\theta \sum_{l=1}^{N_s-1} \xi_l \frac{\partial}{\partial \chi_l}, \end{aligned}$$

$$\begin{aligned} S_{\pm,0} &= \frac{1}{\sqrt{N_s}} \mathrm{e}^{\pm i\phi} (\pm i)(i) \cot\theta \left\{ \sum_{l=0}^{N_s-1} \chi_l \frac{\partial}{\partial \chi_l} - \chi_0 \frac{\partial}{\partial \chi_0} \right\} \\ &= \mp \frac{1}{\sqrt{N_s}} \mathrm{e}^{\pm i\phi} \cot\theta \sum_{l=1}^{N_s-1} \chi_l \frac{\partial}{\partial \chi_l}, \end{aligned}$$

$$Q_{\pm,0} + R_{\pm,0} + S_{\pm,0} = \frac{1}{\sqrt{N_s}} \mathrm{e}^{\pm i\phi} \sum_{l=1}^{N_s-1} \left\{ i\chi_l \frac{\partial}{\partial \xi_l} - i \csc^2\theta \xi_l \frac{\partial}{\partial \chi_l} \mp \cot\theta \chi_l \frac{\partial}{\partial \chi_l} \right\}. \tag{57}$$

Hereafter we use $\tilde{\xi}_l$ and η_l instead of the variables ξ_l and χ_l,

$$\tilde{\xi}_l \equiv \xi_l,\ \eta_0 \equiv \chi_0,\ \eta_l \equiv \chi_l \sin\frac{\xi_0}{\sqrt{N_s}} = \chi_l \sin\theta\ (l \geq 1). \tag{58}$$

Then

$$\frac{\partial}{\partial\chi_0}=\sum_{k=0}^{N_s-1}\left\{\frac{\partial\tilde{\xi}_k}{\partial\chi_0}\frac{\partial}{\partial\tilde{\xi}_k}+\frac{\partial\eta_k}{\partial\chi_0}\frac{\partial}{\partial\eta_k}\right\}=\frac{\partial}{\partial\eta_0},\quad \frac{\partial}{\partial\chi_l}=\sin\theta\frac{\partial}{\partial\eta_l}\quad (l\geq 1),$$

$$\frac{\partial}{\partial\xi_0}=\sum_{k=0}^{N_s-1}\left\{\frac{\partial\tilde{\xi}_k}{\partial\xi_0}\frac{\partial}{\partial\tilde{\xi}_k}+\frac{\partial\eta_k}{\partial\xi_0}\frac{\partial}{\partial\eta_k}\right\}=\frac{\partial}{\partial\tilde{\xi}_0}+\frac{1}{\sqrt{N_s}}\cot\theta\sum_{k=1}^{N_s-1}\eta_k\frac{\partial}{\partial\eta_k},$$

$$\frac{\partial}{\partial\xi_l}=\frac{\partial}{\partial\tilde{\xi}_l}\quad (l\geq 1). \tag{59}$$

With these variables we obtain the approximate expression of $\hat{L}_{\xi,\pm,0}$ in (53),

$$\hat{L}_{\xi,\pm,0}\sim\frac{1}{\sqrt{N_s}}\hat{L}_{A\pm},$$

$$\hat{L}_{A\pm}\equiv e^{\pm i\phi}\left\{\pm\frac{\partial}{\partial\theta}+i\cot\theta\frac{\partial}{\partial\phi}+i\csc\theta\sum_{l=1}^{N_s-1}\left(\eta_l\frac{\partial}{\partial\tilde{\xi}_l}-\tilde{\xi}_l\frac{\partial}{\partial\eta_l}\right)\right\}. \tag{60}$$

Here we find that $\hat{L}_{A\pm}$ and $\hat{L}_\phi=-i\partial/\partial\phi$ are new generators of SU(2),

$$\left[\hat{L}_{A\pm},\hat{L}_\phi\right]=\mp\hat{L}_{A\pm},\ \left[\hat{L}_{A+},\hat{L}_{A-}\right]=2\hat{L}_\phi. \tag{61}$$

Using (60) we have

$$\frac{1}{2}\left(\hat{L}_{\xi,+,0}\hat{L}_{\xi,-,0}+\hat{L}_{\xi,-,0}\hat{L}_{\xi,+,0}\right)\sim\frac{1}{N_s}\left\{\frac{1}{2}\left(\hat{L}_{A+}\hat{L}_{A-}+\hat{L}_{A-}\hat{L}_{A+}\right)\right\}. \tag{62}$$

For $j\geq 1$, $Q_{\pm,j}$, $R_{\pm,j}$ and $S_{\pm,j}$ are negligible compared to $Z_{\pm,j}$ so that $\hat{L}_{\xi,\pm,j}$ is approximated by

$$\hat{L}_{\xi,\pm,j}\sim Z_{\pm,j}=e^{\pm i\phi}\left(\pm\frac{\partial}{\partial\xi_j}+i\cot\theta\frac{\partial}{\partial\chi_j}\right). \tag{63}$$

Then we obtain

$$\frac{1}{2}\sum_{j=1}^{N_s-1}\left(\hat{L}_{\xi,+,j}\hat{L}_{\xi,-,j}+\hat{L}_{\xi,-,j}\hat{L}_{\xi,+,j}\right)\sim-\sum_{j=1}^{N_s-1}\left\{\frac{\partial^2}{\partial\xi_j^2}+\cot^2\theta\frac{\partial^2}{\partial\chi_j^2}\right\}. \tag{64}$$

A2. Reason Why $J\geq|m_\tau|$ in $N_s=2$ Case with Large B

In this subsection we present the reason why J should be greater than or equal to $|m_\tau|$ in (48). Let us denote the wave function for the Hamiltonian $\hat{H}_{A,2}=\hat{H}_L+\hat{H}_O$ by $\Psi_{J,M,n_\rho,m_\tau}(\theta,\phi,\tau,\rho)$. First note that $\hat{H}_L$, $\hat{H}_O$, $\hat{L}_\phi$ and $\hat{L}_\tau$ defined in Subsection 5.1 commute with each other,

$$\left[\hat{H}_L,\hat{H}_O\right]=0,\ \left[\hat{H}_L,\hat{L}_\phi\right]=0,\ \left[\hat{H}_L,\hat{L}_\tau\right]=0,$$

$$\left[\hat{H}_O,\hat{L}_\phi\right]=0,\ \left[\hat{H}_O,\hat{L}_\tau\right]=0,\ \left[\hat{L}_\phi,\hat{L}_\tau\right]=0. \tag{65}$$

Then this wave function with quantum numbers J, M, n_ρ and m_τ satisfies

$$\hat{H}_L\Psi_{J,M,n_\rho,m_\tau}(\theta,\phi,\tau,\rho)=\frac{1}{2}J(J+1)\Psi_{J,M,n_\rho,m_\tau}(\theta,\phi,\tau,\rho),$$

$$\hat{H}_O\Psi_{J,M,n_\rho,m_\tau}(\theta,\phi,\tau,\rho)=2\sqrt{2B}(1+n_\rho)\Psi_{J,M,n_\rho,m_\tau}(\theta,\phi,\tau,\rho),$$

$$\hat{L}_\phi\Psi_{J,M,n_\rho,m_\tau}(\theta,\phi,\tau,\rho)=M\Psi_{J,M,n_\rho,m_\tau}(\theta,\phi,\tau,\rho),$$

$$\hat{L}_\tau \Psi_{J,M,n_\rho,m_\tau}(\theta,\phi,\tau,\rho) = m_\tau \Psi_{J,M,n_\rho,m_\tau}(\theta,\phi,\tau,\rho). \tag{66}$$

From the third and fourth equations in (66) we have

$$\Psi_{J,M,n_\rho,m_\tau}(\theta,\phi,\tau,\rho) = f_{J,M,m_\tau}(\theta) g_{n_\rho,m_\tau}(\rho) \mathrm{e}^{iM\phi} \mathrm{e}^{im_\tau\tau}. \tag{67}$$

By $\hat{L}_{A+,2}$, on the other hand, the eigen function of ϕ with eigen value M changes to that with $M+1$, while the eigen function of τ with eigen value m_τ does not change. Then we obtain the equation for $f_{J,J,m_\tau}(\theta)$ since there exists no $M = J+1$ state,

$$\begin{aligned}
&\hat{L}_{A+,2}\left\{ f_{J,J,m_\tau}(\theta) g_{n_\rho,m_\tau}(\rho) \mathrm{e}^{iJ\phi} \mathrm{e}^{im_\tau\tau} \right\} \\
&= \mathrm{e}^{i\phi}\left\{ \frac{\partial}{\partial\theta} - \cot\theta \hat{L}_\phi - \csc\theta \hat{L}_\tau \right\}\left\{ f_{J,J,m_\tau}(\theta) g_{n_\rho,m_\tau}(\rho) \mathrm{e}^{iJ\phi} \mathrm{e}^{im_\tau\tau} \right\} \\
&= g_{n_\rho,m_\tau}(\rho) \mathrm{e}^{i(J+1)\phi} \mathrm{e}^{im_\tau\tau} \left\{ \frac{\mathrm{d}f_{J,J,m_\tau}}{\mathrm{d}\theta} - \left(J\cot\theta + m_\tau \csc\theta \right) f_{J,J,m_\tau} \right\} = 0.
\end{aligned} \tag{68}$$

The solution is given by

$$f_{J,J,m_\tau}(\theta) = C\left(\sin\frac{\theta}{2} \right)^{J+m_\tau} \left(\cos\frac{\theta}{2} \right)^{J-m_\tau}. \tag{69}$$

Since we need that the solution (69) is finite, we have the condition that $J+m_\tau \geq 0$ as well as $J-m_\tau \geq 0$.